Linear collider physics: effects of changing detector ECAL geometries

G W Murdoch

School of Physics and Astronomy, Kelvin Building, University of Glasgow, Glasgow, G12 8QQ, Scotland, United Kingdom

E-mail: 0900886m@student.gla.ac.uk

Abstract. Full simulation, reconstruction and analysis of the Higgs production process $e^+e^- \to HZ \to b\bar{b}e^+e^-$ at the Compact Linear Collider at a centre-of-mass energy of 350GeV was performed. The effect of changing the geometry of the International Large Detector concept model utilising a silicon layered electromagnetic calorimeter (ECAL) was investigated. A cost-performance analysis for two particle flow algorithms suggested that cost savings of 13% and 33% made on the ECAL would result in a loss of resolution in Higgs mass reconstruction of 20% and 39% respectively, however, resolution could be improved by a factor of 2 using the more sophisticated particle reconstruction algorithm

1. Linear colliders

The proposed linear colliders, the International Linear Collider (ILC) and Compact Linear Collider (CLIC), will carry out experiments to improve on findings made at the LHC, the highest energy particle collider in the world. Since its first proton-proton collisions in 2009[1], LHC physics studies have been at the forefront of particle physics, for example, the Higgs boson discovery[2][3]. An experimental route which is now important to look at in the high energy frontier is the collisions of electrons with their anti-particles, positrons. These fundamental leptons will provide a clean collision environment unlike the environment at the LHC which collides composite particles. The desire to experiment with these light, fundamental particles raises the complication of synchrotron radiation. The LHC is a circular collider therefore a drawback is that synchrotron radiation is emitted due to particles being accelerated in order to follow the circular trajectory. The LHC runs experiments with heavy particles such as protons, whereas to experiment with electrons and positrons, the high continuous energy loss through synchrotron radiation significantly limits the collision energies achievable at the circular collider since this energy loss per complete turn is inversely proportional to m^4, where m is the particle's mass[4]. This is the central motivation for a new linear collider to study electron-positron collisions in a high centre-of-mass (CM) energy range allowing further important physics research to be carried out. At these e^+e^- colliders, the initial-state polarisations are known precisely and can be controlled to alter various production cross-sections[5]. Another benefit is the backgrounds are much lower than QCD backgrounds at hadron colliders[6].

The highest CM energy ($\sqrt{s}$) for lepton collisions ever achieved at a linear collider was $\sqrt{s}$ = 209GeV, achieved at the Large Electron-Positron Collider (LEP) which completed its operation in 2000[7][8].

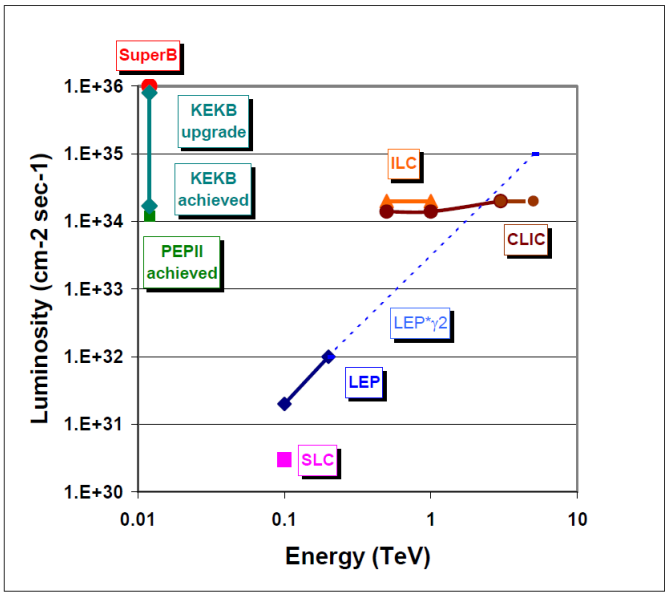

Figure 1: Luminosity versus energy of past, current and future lepton collider projects[12].

A major area of interest is the further study of the Higgs boson. The cross section of different Higgs production processes varies with the CM energy[9], therefore it is desirable to operate a linear collider at different CM energies to provide wide-ranging datasets, with the ultimate goal of operating at the high energy frontier.

2. Linear colliders: the ILC and CLIC

The two main proposed linear colliders utilise different accelerating technologies. The ILC is based on superconducting radiofrequency main linear accelerators provided by superconducting niobium cavities[6][10], generating a maximum beam energy of 250GeV. CLIC has developed its own two beam accelerator technology which operates at room temperature where parallel particle beams utilise kinetic energy transfer from a high-current and low-energy Drive Beam (100A and 2.5-0.25GeV) to a low-current and high-energy Main Beam (about 1A and 9GeV-1.5TeV)[9][11].

The main difference in these colliders is the beam accelerator approaches, leading to different CM energies. Both colliders opt for staged construction to reach the high energy physics frontier and therefore allow a wide range of areas of study over long-term operation. The ILC proposes 200—500GeV (extendable to 1TeV)[10] as the CM energy range in its lifespan. The LHC's current findings are strong grounds for CLIC to operate at an initial low energy of around 350GeV, most likely increasing to 1.4TeV then finally 3TeV[9]. Both ILC and CLIC aim to provide high luminosity e^+e^- collisions at a higher energy than obtainable at current linear collider facilities or those in the past, illustrated in Figure 1.

The design for the ILC has been underway longer than that of CLIC which has led to the ILC's detector design efforts being the best developed and most suitable for the site-specific design based on the selected Kitakami site[13][14]. The ILC has developed two detector designs, ILD and SiD, which are far advanced in simulations, prototyping and validation[15]. These two detectors are proposed to operate in a push-pull system at the interaction point of the collisions. A major appeal for two experiments is to allow for independent studies at each, leading to cross-checking and verification of results[15], similar to that of the Higgs boson discovery at the ATLAS and CMS experiments at the LHC in 2012. From the well-established physics properties of the ILD and SiD at the ILC, the CLIC design proposal benefits from modified versions of

Table 1: Main detecting technologies and properties of the SiD and ILD[15].

Barrel		
	SiD	ILD
Vertex	Si pixels	Si pixels
Tracker	Si strips	Si strips and Time Projection Chamber as main tracking detector
ECAL	Si pixel-W	W absorber, either SiECAL layered cells or ScECAL layered strips
HCAL	RPC-steel	Fe absorber
Coil	5T	3.5T
Endcap		
	SiD	ILD
Vertex	Si pixels	Si pixels
Tracker	Si strips	Si strips
ECAL	Si pixel-W	W absorber, either SiECAL layered cells or ScECAL layered strips
HCAL	RPC-steel	Fe absorber
LumiCal	Si-W (Si sensor readout)	W absorber (30 Si layers)
BeamCal	Semicon-W	W absorber GaAs readout layers

these detectors supporting operation at its optimal CM energy[9].

The frontiers of physics to be investigated at these proposed high energy linear colliders motivates the desire for high precision detectors with a main focus on jet energy resolution and di-jet mass performance[15] where improvements in highly granular calorimetry and tracking allow for the employment of such detectors. Optimal precision in calorimetry is essential to analyse individual particles, this requires high granularity of the ECAL and hadron calorimeter[15]. The detectors will utilise the developments of Particle Flow Analysis in the reconstruction of fundamental particles in such fine detail where the reconstructions will resemble viewing Feynman diagrams[5].

Common features of both the ILD and SiD detector concepts include silicon (Si) and a great interest in tungsten (W) for its short radiation length and small Molière radius, and its mechanical suitability[15]. Table 1 provides an overview of the main detecting technologies and properties of the SiD and ILD designs including the ECAL, hadron calorimeter (HCAL), magnet coil (Coil), luminosity calorimeter (LumiCal) and beam calorimeter (BeamCal).

The ECAL for the ILD has been developed for two options: silicon layered cells (SiECAL) and scintillator layered strips (ScECAL). The iron based absorber for the ILD's HCAL has been investigated for two different approaches; scintillator tiles and gaseous devices. Relevant studies carried out for CLIC use adapted versions of the SiD and ILD — the CLIC_SiD and CLIC_ILD — where the magnetic fields have been optimised to 5T and 4T respectively[9]. Although tungsten is a desirable absorber for the SiD, the decision for a steel HCAL is based on cost constraints which make it unable to justify the modification to the HCAL.

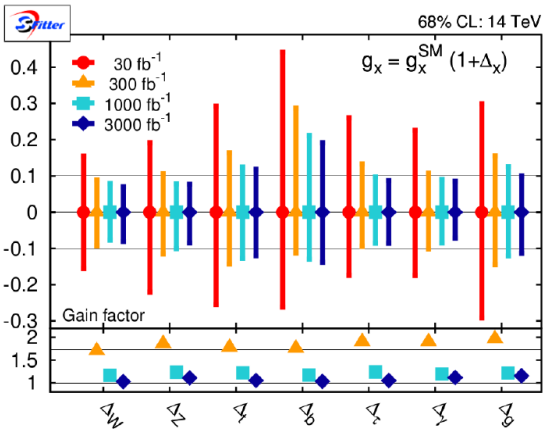

Figure 2: Anticipated precision of the LHC experiments to Higgs boson couplings in a model-independent study, containing all data from operation at $\sqrt{s} = 14$TeV[5].

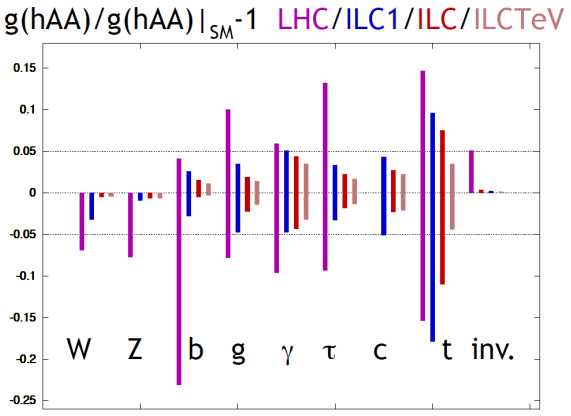

Figure 3: Estimated precision to Higgs boson couplings in a model-independent study at the LHC and ILC. 1σ confidence intervals are displayed for LHC at 14TeV with 300fb^{-1}, ILC at 250GeV with 250fb^{-1}('ILC1'), ILC at 500GeV with 500fb^{-1} ('ILC') and with 1000fb^{-1} for the final upgrade of ILC at 1TeV ('ILCTeV'). The horizontal band signifies a 5% deviation from the SM prediction for the Higgs coupling[21].

3. Comparison of the ILC and CLIC to the LHC and HL-LHC

The overall timeframe for the proposed linear colliders spans decades; for example, CLIC still has to complete its development phase, preparation phase and construction phase with planned commissioning from 2030[16]. This CLIC commissioning would tie in with the conclusion of the longest-term proposed planned LHC operation (including the proposal of the High Luminosity LHC (HL-LHC) upgrade). The ILC is further along than CLIC in its development, having published a comprehensive Technical Design Report as opposed to CLIC's Conceptual Design Report. An estimate for the ILC's construction and commissioning is 8 years[17], similar to that of CLIC. The timeframe of the LHC and its proposed upgrades should be considered to appreciate those of the ILC and CLIC, where they look to compliment and further the LHC studies. The LHC is currently in its first long shutdown phase (LS1) and will be operating from 2015 at its optimal CM energy of 14TeV[18] with no confirmed operation after this stage. There are two more proposed long shutdown phases (LS2 and LS3) to achieve the HL-LHC to continue experiments up until approximately 2030[18]. Due to the long-term nature of these colliders it is useful to not only compare ILC with CLIC but to also assess the LHC and LHC upgrades.

The HL-LHC aims to achieve a luminosity of $L = 5\text{x}10^{34}\text{cm}^{-2}\text{s}^{-1}$ and integrated luminosity of 250fb^{-1} per year from 2022 with the objective to obtain 3000fb^{-1} by approximately 2030[19] [20]. From the LHC operation at $\sqrt{s} = 14$TeV in 2015 until the end of HL-LHC operation, an estimation of the precision of Higgs boson couplings in a model-independent analysis is displayed in Figure 2. There is a gradual improvement in these sensitivities over the course of operation at the $\sqrt{s} = 14$TeV LHC, including its potential upgrades. Comparing Higgs couplings sensitivities is most beneficial as this is a key area of focus for collider technologies for the foreseeable future.

Figure 2 shows that most of the sensitivities do not significantly improve over the course of the integrated luminosity increase from 1000fb^{-1} to 3000fb^{-1} which corresponds to 8 years operation of the HL-LHC. Figure 3 displays the comparison of sensitivities possible at the ILC

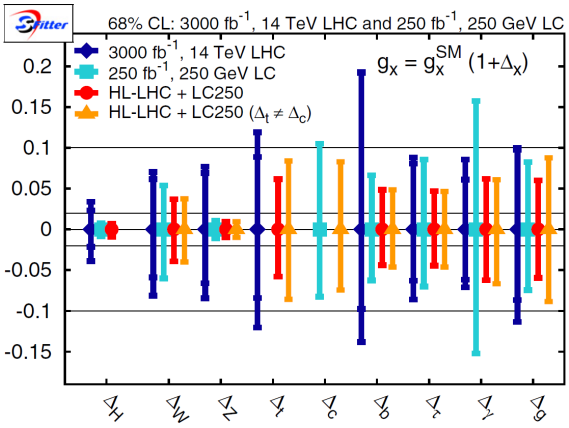

Figure 4: Anticipated accuracy for Higgs coupling at the HL-LHC, the ILC at $\sqrt{s} =$ 250GeV, including their combination. The case where the Htt coupling is anomalous is shown separately ($\Delta_t \neq \Delta_c$). The inner bars for HL-LHC (3000fb^{-1}, 14TeV LHC) represent a situation with improved systematic uncertainties[22].

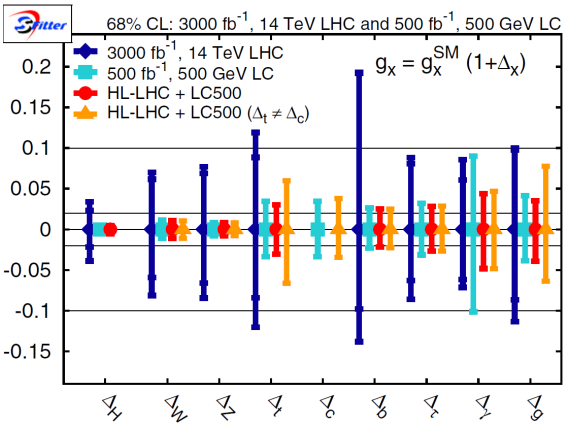

Figure 5: Anticipated accuracy for Higgs coupling at the HL-LHC, the ILC at $\sqrt{s} =$ 500GeV, including their combination. The case where the Htt coupling is anomalous is shown separately ($\Delta_t \neq \Delta_c$). The inner bars for HL-LHC (3000fb^{-1}, 14TeV LHC) represent a situation with improved systematic uncertainties[22].

over its staged CM energy plan and highlights a motivation for its construction in the context of Higgs physics. Figure 3 demonstrates with the ILC operating at $\sqrt{s} = 500$GeV, all Higgs boson couplings are more precise than compared with the LHC before the upgrade to the HL-LHC. There would be approximately a ten year gap between the end of LHC measurements and the first measurements at the ILC operating at $\sqrt{s} = 250$GeV, hence there is a strong case for the HL-LHC so more precise physics experiments can be carried out in this vacant period.

Evaluating the potential results from operating the HL-LHC before the ILC establishes that there is a great complementarity between the colliders in the study of Higgs boson couplings post $\sqrt{s} = 14$TeV LHC. Figures 4 and 5 highlight the substantial benefit of the ILC to improve on the expected sensitivities of the LHC and HL-LHC, however, the values are not included for the ILC operation at 1TeV. The linear collider sensitivities dominate the combination with the HL-LHC values, demonstrating its powerful capabilities in achieving better Higgs couplings measurements[22]. It should be noted that the most accurate couplings can be determined with the combination of results at both HL-LHC and ILC than at any individual collider[22].

Table 2 and Table 3 display the Higgs couplings measurement capabilities at the ILC and CLIC respectively, showing similarities with significant improvements in the TeV energy range.

4. Linear collider experiments

The high precision capabilities and clean environment e^+e^- collisions at the linear collider further motivate Standard Model (SM) and Beyond Standard Model (BSM) physics studies. The key focus is more accurate Higgs couplings measurements due to the fact that deviations from the boson's couplings in the range of 5-10% would lead towards a new physics model due to the nonconformity with the SM[5]. This is evidently further motivation for extensive research of the Higgs boson discovered in 2012 as many extended Higgs theories include a Higgs scalar with very similar properties to the SM Higgs boson[6].

Table 2: Anticipated precisions of Higgs couplings and total Higgs width at the ILC. "-" denotes values which cannot be quantified with adequate precision at the given CM energy. The estimated values correspond to the canonical scenario outlined in [23] which includes the estimation for the recent study of a luminosity upgraded scenario at the ILC[23].

parameter	250GeV	250GeV + 500GeV	250GeV + 500GeV + 1TeV
g_{HZZ}	1.3%	1.3%	1.3%
g_{HWW}	4.8%	1.4%	1.4%
g_{Hbb}	5.3%	1.8%	1.5%
g_{Hcc}	6.8%	2.9%	2.0%
g_{Hgg}	6.4%	2.4%	1.8%
$g_{H\tau\tau}$	5.7%	2.4%	1.9%
$g_{H\gamma\gamma}$	18%	8.4%	4.1%
$g_{H\mu\mu}$	-	-	16%
g_{Htt}	-	14%	3.2%
Γ_H	11%	5.9%	5.6%

Table 3: Anticipated precisions of Higgs couplings and total Higgs width at CLIC. "-" denotes values which cannot be quantified with adequate precision at the given CM energy while values marked "<" have not yet been investigated at the given CM energy, but should result in a substantial improvement in the precision. For the $\sqrt{s}$ = 3TeV value of g_{Htt}, less of an improvement is anticipated due to reduced cross-section at this higher energy, however it has not yet been investigated[24].

parameter	350GeV	350GeV + 1.4TeV	350GeV + 1.4TeV + 3TeV
g_{HZZ}	2.1%	2.1%	2.1%
g_{HWW}	2.6%	2.1%	2.1%
g_{Hbb}	2.8%	2.2%	2.1%
g_{Hcc}	3.8%	2.4%	2.2%
g_{Hgg}	4.1%	2.3%	2.2%
$g_{H\tau\tau}$	4.0%	2.5%	<2.5%
$g_{H\gamma\gamma}$	-	5.9%	<5.9%
$g_{H\mu\mu}$	-	11 %	5.6%
g_{Htt}	-	4.5%	∼4.5%
Γ_H	9.2%	8.5%	8.4%

Higher precision physics with regards to gauge bosons and new particles is another crucial area of investigation at a linear collider. One domain of BSM physics to explore is the potential of pair-production of colour-neutral states at a linear collider since the discovery reach is much greater than the LHC with regards to this pair-production[6]. The search for supersymmetry is another important exploration in BSM physics.

The Higgs sector at linear colliders is comprised of many areas due to the fact that through the staged implementation of CM energy operation, different production mechanisms and branching ratios can be examined in great detail.

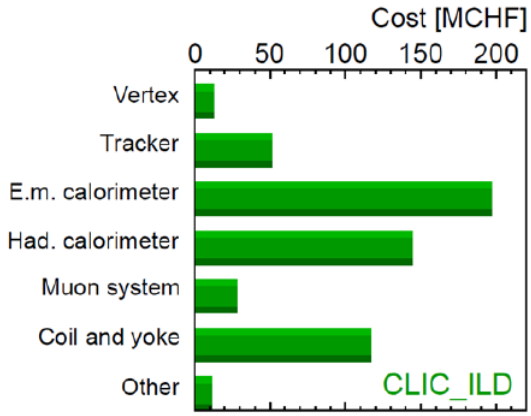

Figure 6: Breakdown of cost of the CLIC_ILD which utilises the SiECAL model. Value in standardised CLIC study units[25].

5. Project aim

Extensive research into both CLIC and ILC is still on-going since both have the capability to complement and exceed the physics potential of the LHC and HL-LHC and continue important high energy physics studies beyond the 2020's. CLIC still has to publish technical design reports[11], whereas the ILC has reached this stage in its development. However, technology choices have not yet been made for the ILC, where there is the possibility that the two detector system will be abandoned to opt for just one detector which may be some adaptation of both the ILD and SiD detectors, in the pursuit of reducing costs —a major constraint.

Developing a means of assessing detector choices to compare different options is invaluable. With on-going silicon technology advancements, this detector analysis would allow a convenient way to examine the capabilities having changed specific detector geometries at the linear collider facility. Examining the different implementations of silicon pixels and strips in the ILD and SiD is one important geometry modification requiring investigation due to developing silicon technology capabilities. Monitoring the detector performance and sensitivities is a crucial part of the research and development of the accelerator projects, possibly suggesting new approaches or justifying an existing detector structure. Building the capability to conduct these studies effectively will be critical in the progress of these linear collider projects.

6. ECAL studies

This investigation focused on changing the structure of the ECAL to perform cost-performance analysis. This study utilises the CLIC_ILD_CDR500 detector model which uses a silicon layered ECAL model (SiECAL), with corresponding relative costs shown in Figure 6. ECAL changes were considered for this model since they are, by far, the most expensive subdetector component of the CLIC_ILD detector. The ECAL corresponds to approximately 35% of the total cost shown in Figure 6.

The ECAL is comprised of tungsten absorber strips, active silicon elements, support and electronic materials. The effect on resolution was examined only for alterations of the geometry of the tungsten strips. The ECAL has 3 subsections: EcalBarrel, EcalEndcap and EcalPlug (situated at the endcap). The absorber layer thickness changes made in ECAL parameters were simultaneously applied to each of these ECAL subsections. The ECAL encases the TPC (time projection chamber) which is the first detector component surrounding the interaction point in the detector, illustrated in Figure 7a. The ECAL covers as much volume as practicably possible with its three subsections for the crucial measurements of the energy of particles interacting

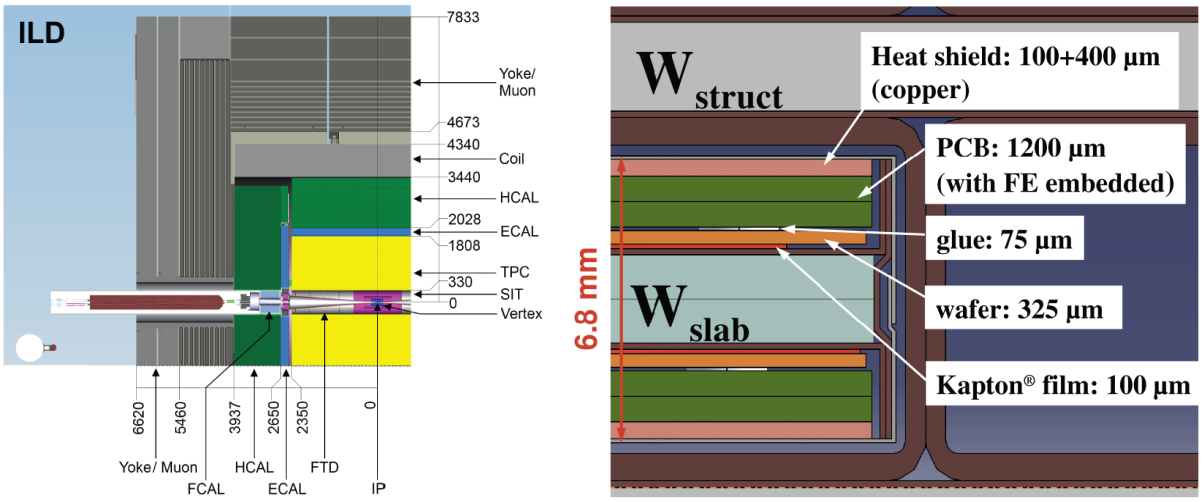

(a) Quadrant view of the ILD with the interaction point (IP) in the lower right corner. Dimensions given are in mm[26].

(b) Cross section through the SiECAL. The silicon layer is labeled 'wafer' and surrounds the W slab[26].

Figure 7: Illustrations of the geometry of the ILD detector and SiECAL at CLIC.

Table 4: ECAL parameters used in this investigation. The default 30 layer model and the two modified versions are described.

ECAL Model	W Layers	Absorber Layer Thickness
30 Layers	20	2.1mm
	9	4.2mm
26 Layers	17	2.4mm
	8	4.8mm
20 Layers	13	3.15mm
	6	6.3mm

predominantly via the electromagnetic interaction. The default ILD SiECAL model consists of 30 layers in which there are 30 silicon layers and 29 tungsten absorber strips. Figure 7b illustrates the ECAL geometry for one tungsten layer. Table 4 outlines the basic structure of the default SiECAL model and the modified versions used in the investigation. The basic geometry consists of 2 stacks of tungsten layers with a ratio of approximately 2:1 in layers in the stacks, and 1:2 in absorption layer thickness. This geometry arrangement in which only the layers and absorber thickness are changed is important in the analysis of physics measurements with the implementations of these detector models. Investigation of using coarser tungsten layers leads to a reduction in cost as there is less silicon, support and electronic materials, but at the expense of performance in physics measurements which is obviously the interest in such research[27].

Approximately half of the hadronic particle showers begin in the ECAL therefore high granularity is imperative for operation at the collider for proficient cluster separation, therefore achieving precise measurements[26][28].

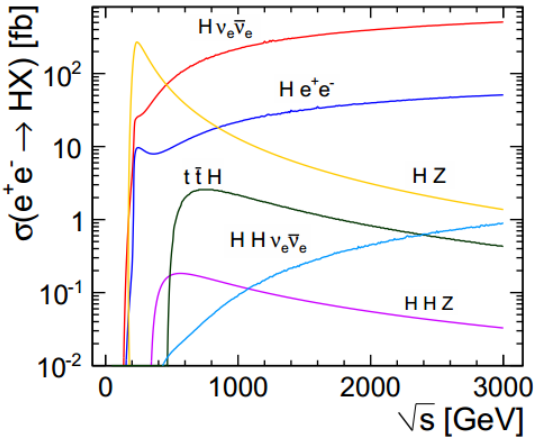

(a) Higgs cross-section production mechanisms as a function of CM energy[29].

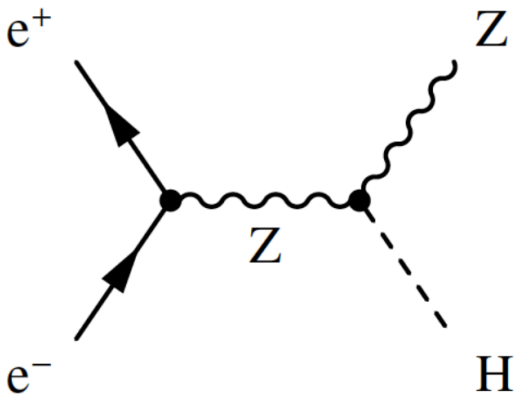

(b) Higgs-strahlung is the dominant production mechanism for $\sqrt{s} = 350$GeV[30].

Figure 8: Production mechanisms examined for CLIC operating at $\sqrt{s} = 350$GeV.

7. Project method

7.1. Higgs-strahlung channel

The investigation focused on the analysis of Monte Carlo (MC) generated events at a CM energy of 350GeV which is the first proposed stage of CLIC operation.

At $\sqrt{s} = 350$GeV the dominant Higgs production channel is the Higgs-strahlung channel shown in Figures 8a and 8b. This study focuses on the case of Z decaying to an electron and a positron:

$$e^+e^- \rightarrow HZ \rightarrow H(Z \rightarrow e^+e^-)$$

The Higgs branching ratio depends on the mass of the Higgs, which is 120GeV in this study, such that the dominant decay is $H \rightarrow b\bar{b}$ with corresponding branching ratio of 0.648 ± 0.018 [31]. This dominant decay of the Higgs boson was investigated.

Direct reconstruction of the Z and H boson was carried out from their daughter particles and jets, respectively.

7.2. Software

The overview of the method is simulating, reconstructing and analysing MC generated events of the specified Higgstrahlung channel.

Software packages for a linear collider - ILCSoft[32] - were utilised in the process:

- Marlin is the C++ software framework for the whole process, used in analysis and reconstruction code.
- Mokka provides GEANT4-based full simulations and uses realistic descriptions of detectors for these CLIC based simulations.
- MarlinReco deals with the reconstruction of raw data, which includes jet reconstruction such as the WOLF particle flow processor.
- MarlinPandora is the ILD Pandora client application which is the particle flow algorithm (PFA) based on PANDORAPFANew[33].
- The LCFI software was used for flavour identification of jets for reconstruction.

As part of this project, the full detector simulation and reconstruction was made to work for the first time in Glasgow, and all simulated data was generated within the project.

Simulations for the three different detector geometries described in Table 4 used the same Monte Carlo data, providing a like for like analysis for 10,000 events.

Mokka was used to change the tungsten absorption layer thickness and number of layers as constructed by GEANT4.

7.3. Particle flow algorithms

The concept of particle flow is a new paradigm in particle physics experiments, based on the idea that individual particles may be tracked and reconstructed through very finely-grained detectors.

CLIC detectors require high jet energy resolution, leading to excellent energy and mass resolutions which particle flow algorithms (PFAs) can achieve. Both WOLF and PANDORAPFANew are PFA frameworks utilising clusters and tracks for the reconstruction and identification of particles.

The WOLF and PANDORA PFAs execute sophisticated pattern recognition processes by utilising reconstructed tracks from the detector's tracking systems and energy deposits ('clusters') in the ECAL and HCAL. Proximity cuts are applied in addition to the geometric analysis carried out when extrapolating tracks into the calorimeter and associating them to clusters.

8. Wolf PFA

8.1. Method

The reconstruction technique for analysis in the Higgs-strahlung channel required track digitisation, tracking performed with this information, the PFA to be applied and finally jets reconstructed and truth tagged, all using ILCSoft processors with default parameters.

Firstly the tracker hit digitisation was performed for the silicon tracking systems (SET, SIT and FTD), the vertex system (VTX) and TPC. The track collection was then created from the tracker hit digitisation. Simple digitisation was performed for the calorimeter hits in both the ECAL and HCAL. Track-wise clustering was then executed using the track collection and the ECAL and HCAL collections. The WOLF PFA processor then created reconstructed particles from matching the clusters to TPC tracks and then identified the particle based on the fraction of energy measured in the ECAL and HCAL[34][35]. Jets were created by the Satoru Jet Finder processor from the reconstructed particles before finally determining the true flavour of these jets using the corresponding MC particles.

Additional requirements and cuts were made in the analysis to find the most likely candidates for the reconstruction of the Z and H bosons, for example, examination and cuts on a particle's pseudo rapidity, energy, charge and particle ID.

8.2. Z reconstruction

The first reconstruction performed in the analysis is that of the Z boson - directly reconstructed from its most likely daughter candidate particles (electron and positron). The 'raw' electron energy measured in the ECAL is displayed in Figure 9a. It highlights the staggered peaks for the different ECAL models which is due to the fact that there is less distance in which the energy of the particle can be deposited and a recalibration of the algorithm is required (described later).

The WOLF PFA reconstructs objects that correspond to the MC generated particles in the event, therefore an energy resolution plot in Figure 9b illustrates the efficiency of WOLF's electron reconstruction. This figure shows a relatively small peak near 0 indicating very poor reconstruction of the electron; however, this is very rare as 10,000 events were analysed.

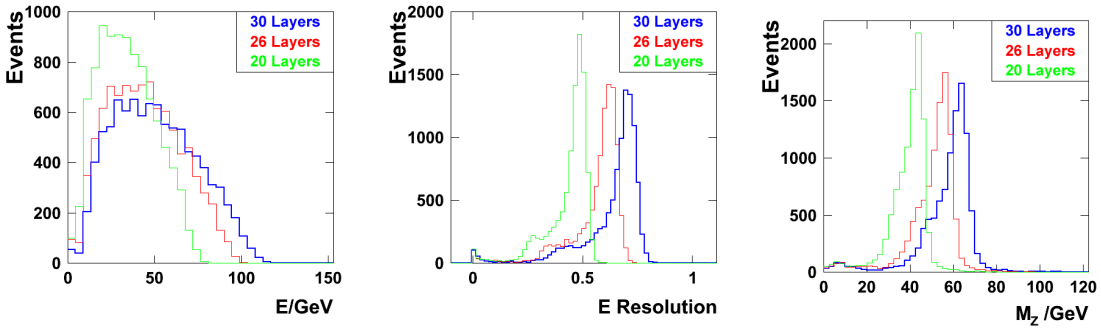

(a) ECAL cluster energy used in the WOLF reconstruction of the Z daughter e^-.

(b) Energy resolution obtained for WOLF reconstructed e^- / MC generated e^-.

(c) WOLF reconstructed Z mass. All models show a lower mass peak than anticipated.

Figure 9: Z daughter e^- ECAL information and Z reconstruction plots for the three different ECAL thicknesses. Coarser tungsten ECAL models show a significant offset.

Table 5: Energy scaling factors to be implmented in the Z reconstruction. Mean values relating to e^- energy resolution (Figure 9b).

ECAL Model	Mean	Energy Scaling Factor
30 Layers	0.72	1.388888889
26 Layers	0.63	1.587301587
20 Layers	0.49	2.040816327

The invariant mass of the reconstructed Z boson was determined from the daughter electron and positron particles, where Figure 9c shows a somewhat successful first attempt for all ECAL models but all have a much lower peak than what is expected. The Z mass is known to be 91.188GeV therefore energy scaling was required to improve the Z reconstruction.

8.3. Z reconstruction with energy scaling

Energy scaling factors shown in Table 5 were determined from the energy resolution plot, Figure 9b. The scaling factors were utilised to obtain the energy resolution with a peak centred at 1 for each of the ECAL models.

This energy scaling successfully aligns these such that they show an energy resolution peak at ∼0.99 for each of the ECAL models, illustrated in Figure 10a. Degradation in resolution can be seen for the coarser ECAL layer models such that the peak shape in this 0.99 region is wider (evident from the height of the peak).

A far better reconstructed Z mass was obtained after using energy scaling, displayed in Figure 10b. Again this resolution degradation for the modified ECAL models is clearly evident for the mean of ∼89GeV.

To quantify the loss in resolution, an estimation of best fitting a Gaussian function in a specified range at the mass peak obtained the measurements in Table 6. The 26 layer model shows a loss in resolution of 5%, and the 20 layer model shows a loss of 16%.

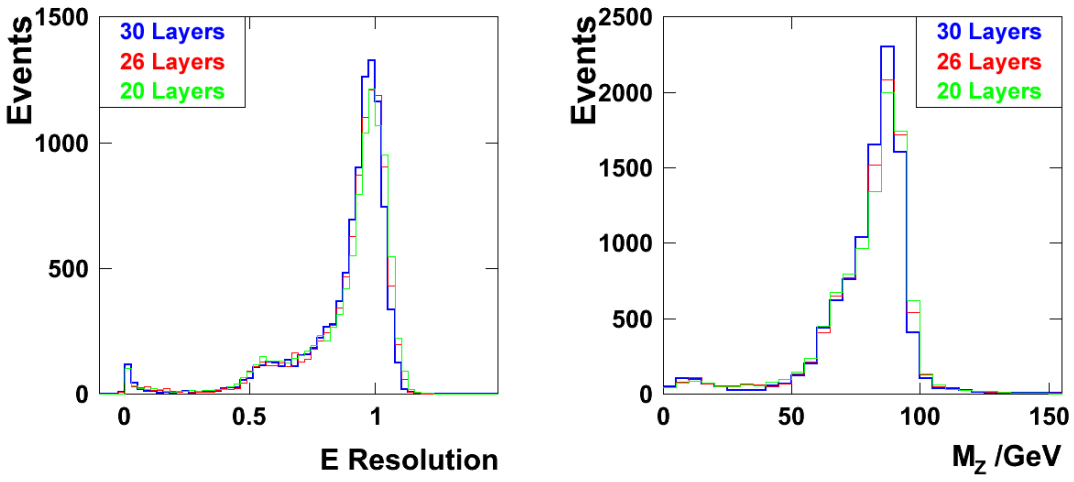

(a) Energy resolution obtained for WOLF e^- / MC e^-.

(b) WOLF reconstructed Z mass.

Figure 10: Implementation of energy scaling factors improves Z reconstruction.

Table 6: WOLF Z reconstruction resolution determined from Figure 10b

ECAL Model	Sigma/Mean
30 Layers	0.0517
26 Layers	0.0543
20 Layers	0.0602

8.4. H reconstruction

The Higgs reconstruction was different from the Z reconstruction such that it required the implementation of jet finder techniques to determine the most likely daughter candidate particles in the dominant decay of $H \rightarrow b\bar{b}$. Similar analysis to the Z reconstruction implies firstly looking at the energy resolution of the tagged b-jets to the MC particles, Figure 11a, and determining the invariant mass of the H boson using direct reconstruction, Figure 11b.

Energy scaling was obviously required for the b-jet reconstruction to improve H reconstruction.

8.5. H reconstruction with energy scaling

The necessary energy scaling factors in Table 7 were obtained from the energy resolution plot, Figure 11a.

The energy resolution, Figure 12a, shows a rather significant loss of resolution for the 30 layer ECAL model, where all model peaks are situated at ∼0.97. This leads to the obvious resolution loss in the reconstructed Higgs mass, with mean of ∼119GeV, shown in Figure 12b. All models overlay fairly well but it can be seen that the peak shape for the 20 layer model has a wider tail.

The relevant measurements for quantification of loss in resolutions from the Higgs invariant mass are displayed in Table 8 and establishes a loss of 20% for the 26 layer model and 39% for the 20 layer model.

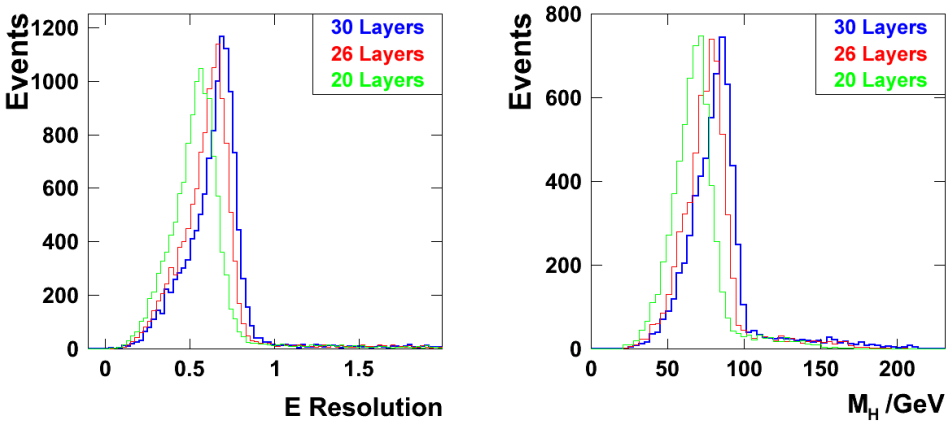

(a) Energy resolution of tagged b-jets / MC b quarks.

(b) Reconstructed Higgs mass.

Figure 11: WOLF Higgs reconstruction using b-jet tagging, for three different ECAL thicknesses. Results indicate energy scaling will be required.

Table 7: Energy scaling factors to be implmented in the H reconstruction. Mean values relating to b-jet energy resolution (Figure 11a).

ECAL Model	Mean	Energy Scaling Factor
30 Layers	0.71	1.408450704
26 Layers	0.67	1.492537313
20 Layers	0.58	1.724137931

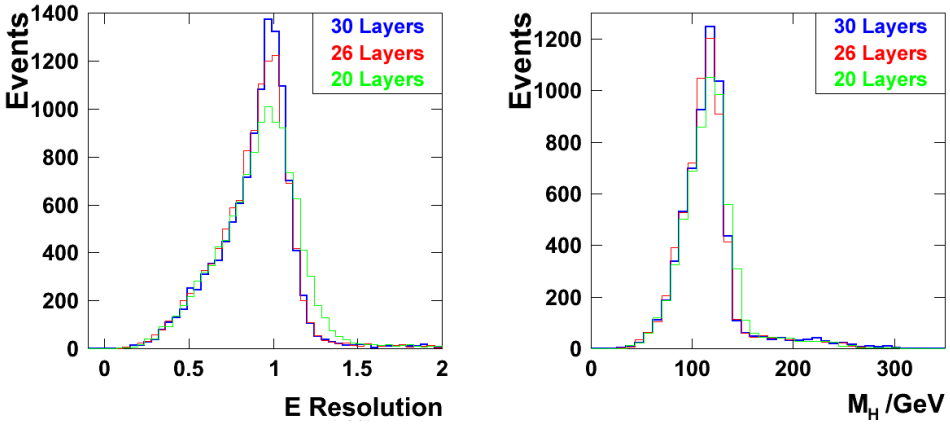

(a) Energy resolution of tagged b-jets / MC b quarks.

(b) Reconstructed Higgs mass.

Figure 12: H reconstruction with energy scaling factors applied.

Table 8: WOLF H reconstruction resolution determined from Figure 12b

ECAL Model	Sigma/Mean
30 Layers	0.0770
26 Layers	0.0925
20 Layers	0.1069

8.6. WOLF PFA conclusion

It is clearly evident from Tables 6 and 8 that the energy resolution degrades more for the b-jets measurements than for the electrons and positrons in the Z reconstruction which is due to the fact that jet reconstruction is more reliant on ECAL measurements of the energy deposited by particles in the decay. Electron and positron reconstruction is mainly from tracking information in the TPC, therefore the modifications to the ECAL has far less of an effect on Z reconstruction.

Although WOLF includes both tracking and clustering in the reconstruction of particles, utilising more information for these processes leads to improved reconstruction and resolution. PANDORA is a more complex and advanced PFA which was also investigated.

9. PANDORA PFA

9.1. Method

Further to WOLF's input collections, PANDORA utilises more information by applying digitisation to more of the silicon tracking system (includes the ETD), the radiation hard calorimetric LHCAL detector, the Muon system, and PANDORA takes vertex collections into account. It is more refined with complex algorithms carried out by the distinct processor which includes both the clustering and formation of the particle flow objects (PFOs)[36][37].

The overall process in the reconstruction of PFOs was the same as for WOLF but with the more sophisticated and supplementary processors for digitisation and tracking. The reconstruction of jets from these PFOs was the same, allowing for a good comparison of H reconstruction.

9.2. Z reconstruction

Again, the 'raw' data of electron energy measured in the ECAL shows a peak shift towards lower energies for the modified ECAL geometries, Figure 13a. However, all peaks are found to be at higher energies than that measured for the WOLF PFA. A vast improvement in the Z electron energy resolution is evident from Figure 13b.

The Z boson invariant mass reconstructed from the PANDORA electron and positron was successfully produced such that no energy scaling was required as there is a clear peak for all ECAL models at $\sim$91GeV, Figure 13c.

9.3. H reconstruction

The energy resolution of the tagged b-jets to the MC particles, Figure 14a, demonstrates that the reconstruction of b-jets from PANDORA PFOs has been better calibrated by the processor than WOLF. Energy scaling was still required for the modified ECAL models to obtain the optimal peak in line with that of the 30 layer model to achieve a more precise Higgs reconstruction than that obtained in Figure 14b.

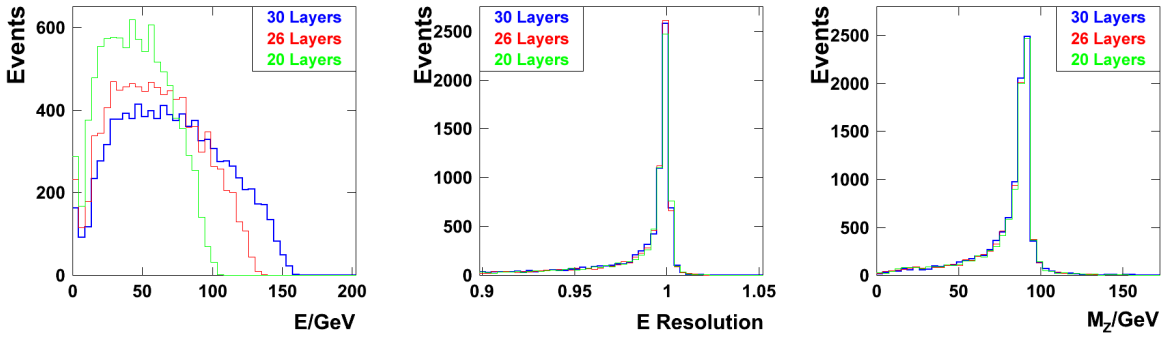

(a) ECAL cluster energy used in the PANDORA reconstruction of the Z daughter e^-.

(b) Energy resolution obtained for PANDORA e^- / MC e^-.

(c) PANDORA reconstructed Z mass.

Figure 13: Plots illustrate the efficiency of corrections applied by PANDORA in the Z reconstruction.

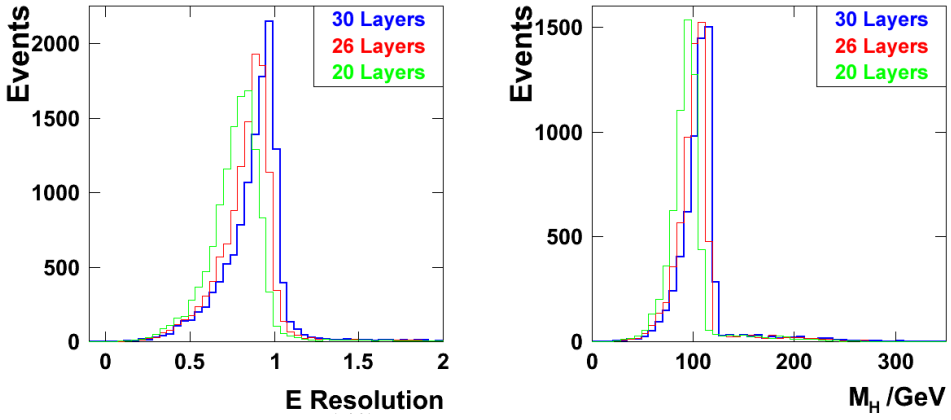

(a) Energy resolution of tagged b-jets / MC b quarks.

(b) Reconstructed Higgs mass.

Figure 14: PANDORA Higgs reconstruction using b-jet tagging. Results indicate energy scaling will be required.

9.4. H reconstruction with energy scaling

Having applied energy scaling factors, the aligned energy resolution (Figure 15a) illustrates the loss in resolution similar to that for the WOLF PFA, where all model peaks are situated at ∼0.96.

The Higgs reconstruction is very well defined for all models for PANDORA, Figure 15b. Again, using the approximation of a Gaussian fit within a region near the peak, the resolution loss can be determined from sigma/mean ratios displayed in Table 9. The loss in resolution in the reconstructed Higgs mass is quantified as 15% for the 26 layer model and 85% for the 20 layer model (a larger degredation than seen for the WOLF algorithm). However, the absolute resolutions are in all cases much better than that obtained using the WOLF algorithm.

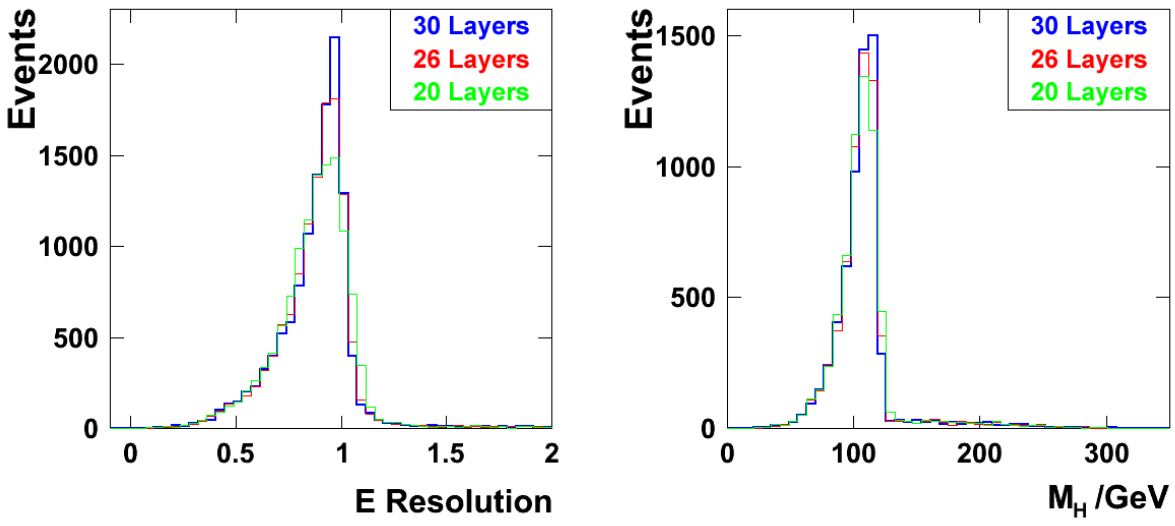

(a) Energy resolution of tagged b-jets / MC b quarks.

(b) Reconstructed Higgs mass.

Figure 15: H reconstruction with energy scaling factors applied.

Table 9: PANDORA H reconstruction resolution determined from Figure 15b

ECAL Model	Sigma/Mean
30 Layers	0.0418
26 Layers	0.0480
20 Layers	0.0774

Table 10: Composition of jets[38].

Particle/carrier	Energy of Jet (%)
Charged particles (mainly hadrons)	62
Photons	27
Long-lived neutral hadrons	10
Neutrinos	1.5

9.5. Composition of jets

Examining the composition of jets can be used to try to understand the effects seen in the reconstructed jet resolution, at a fundamental level. Table 10 quantifies the typical composition of a jet which is important as PFAs only use calorimeter information for photons and neutral particles, as opposed to calculating the momenta of charged particles in tracking detectors[38]. PFAs significantly improve on previous reconstruction techniques where the HCAL measured ∼72% of the jet energy which meant that HCAL granularity was a large limiting factor. PFAs rely on the accurate association of energy in the calorimeters to reconstructed particles.

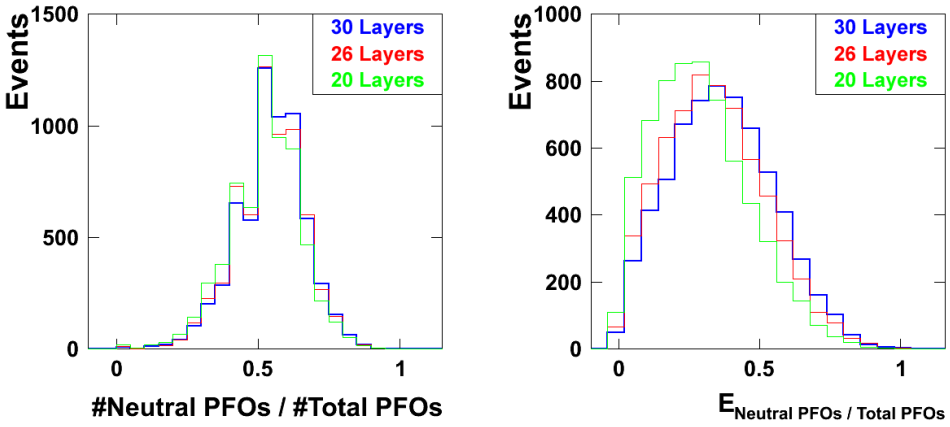

(a) The mean of this ratio decreases for coarser tungsten ECAL models.

(b) The mean of this energy ratio decreases for coarser tungsten ECAL models.

Figure 16: Neutral PFOs information illustrated as a ratio to the total PFOs in the b-jets.

Table 11: Statistics corresponding to the ratio of neutral to total PFOs in the b-jets (Figure 16a).

ECAL Model	Mean	RMS
30 Layers	0.5434	0.1205
26 Layers	0.5364	0.1231
20 Layers	0.5207	0.1263

Table 12: Statistics corresponding to a Gaussian fit between 0 and 1 in Figure 16b.

ECAL Model	Mean	RMS
30 Layers	0.3538	0.1937
26 Layers	0.3194	0.1976
20 Layers	0.2544	0.1992

Figure 16a shows that the ratio of neutral to total PFOs in the b-jets have a peak at 0.5 for all ECAL models, with further statistical information given in Table 11. The mean gradually decreases for the progressively coarser ECAL models indicating poorer identification of these neutral PFOs in the b-jets.

To analyse the energy ratio shown in Figure 16b, a rather poor (but consistent) approximation of applying a Gaussian fit over the whole range of 0 to 1 obtained the mean and RMS statistics quantified in Table 12. The significant decrease in mean values for the energy ratio of neutral to total PFOs in the b-jets indicates that the coarser ECAL models will indeed achieve poorer resolution than the 30 layer model.

10. Implications

Assuming a linear relation between the active silicon and passive tungsten elements in the SiECAL model in the ILD, the saving in ECAL cost when using the 26 and 20 layer options is 13.3% and 33.3%, respectively. As previously discussed, the ECAL is the most expensive detector component (approximately 35% of the total CLIC_ILD cost) therefore the savings would be very significant. The overall saving for the CLIC_ILD would correspond to $\sim$5% for the 26 layer model, and $\sim$12% for the 20 layer model. Cost-performance analysis can help justify which ECAL model to use in the detector.

The resolution loss corresponding to these cost savings was quantified in this study from Higgs reconstruction for both the WOLF and PANDORA PFAs. The resolution loss corresponds to 20% and 39% for WOLF, and 15% and 85% for PANDORA, for the 26 layer and 20 layer ECAL models respectively. Although the loss in resolution is very high for the 20 layer model when using the PANDORA PFA, as an absolute value it is similar to the resolution obtained using the WOLF PFA for the the 30 layer model. This highlights the importance of an advanced PFA as it can lower the impact of degradation of resolution as a result of cost savings.

11. Conclusions

An investigation into the effect that altering ECAL geometries has on the performance of physics measurements has been carried out for simulations at the Compact Linear Collider using two different particle flow algorithms. As anticipated, the coarser tungsten ECAL models led to a loss in resolution but it was found that the choice of PFA greatly influences how much of an effect this loss of resolution is. The results obatined suggest that the more complex and proficient PFA of PANDORA will be the best option to utilise at CLIC.

Acknowledgments

I would like to express my special thanks to Dr Aidan Robson, Project Supervisor, for his support and guidance as well as inspiration and encouragement from start to finish of my project.

I am very grateful to Dr Dan Protopopescu, Project Backup Supervisor, in particular for his work on simulations which were key to my project and also for his guidance and assistance.

References

[1] ALICE Collaboration 2010 First proton-proton collisions at the LHC as observed with the ALICE detector: measurement of the charged-particle pseudorapidity density at $\sqrt{s} = 900$GeV *Eur.Phys.J.* **C65** pp 111-125

[2] ATLAS Collaboration 2012 Observation of a New Particle in the Search for the Standard Model Higgs Boson with the ATLAS Detector at the LHC *Phys. Lett. B* **716** pp 1-29

[3] The CMS Collaboration 2013 Observation of a new boson at a mass of 125 GeV with the CMS experiment at the LHC *Phys. Lett. B* **716** (2) pp 1-30

[4] Willie K 1991 Synchrotron radiation sources *Reports on Progress in Physics* **54** pp 1005-1068

[5] Howard Baer et al 2013 *The International Linear Collider Technical Design Report* vol 2 pp 1-172

[6] Brau J E et al 2012 The Physics Case for an e^+e^- Linear Collider arXiv:1210.0202 [hep-ex] (2) pp 1-15

[7] Kado M M and Tully C G 2002 The Searches for Higgs Bosons at LEP *Annu. Rev. Nucl. Part. Sci.* **52** pp 65-113

[8] Assmann R W et al 2001 *Electron-Positron Collisions at 209 GeV in LEP* 19th IEEE Particle Accelerator Conf. (Chicago) 18-22 June 2001 pp.e-proc. 356

[9] CLIC Detector and Physics Study Collaboration 2013 Physics at the CLIC e^+e^- Linear Collider - Input to the Snowmass process 2013 arXiv:1307.5288 [hep-ex] (3) pp 1-29

[10] Behnke T et al 2013 *The International Linear Collider Technical Design Report* vol 1 pp 1-39

[11] Aicheler M et al 2012 *A Multi-TeV linear collider based on CLIC technology: CLIC Conceptual Design Report* vol 1 pp 1-813

[12] Delahaye J P 2008 *J. Phys.: Conf. Ser.* **110** 012009

[13] Linear Collider Collaboration 2013 ILC candidate site in Japan announced [online] Available at: <http://newsline.linearcollider.org/2013/08/29/ilc-candidate-site-in-japan-announced/> [Accessed 7/11/2013]

[14] ILC Strategy Council Official Website 2013 (Press release) Announcement of the results of the ILC candidate site evaluation in Japan [online] Available at: <http://ilc-str.jp/topics/2013/08281826/> [Accessed 7/11/2013]

[15] Behnke T et al 2013 *The International Linear Collider Technical Design Report* vol 4 pp 1-318

[16] Dannheim D et al 2013 CLIC e^+e^- Linear Collider Studies - Input to the Snowmass process 2013 arXiv:1305.5766 [physics.acc-ph] pp 1-9

[17] Lamont M 2012 LHC Accelerator Prospects [PowerPoint presentation] Sixth LHC Higgs Cross Section Workshop (Zurich) 24-25 May 2012

[18] Zimmermann F 2013 *LHC Status & Plan before HL-LHC* [PowerPoint presentation] CERN/BE Higgs & Beyond Conf. (Sendai) 5 June 2013

[19] Rossi L and Brüning O 2012 High Luminosity Large Hadron Collider A description for the European Strategy Preparatory Group CERN-ATS-2012-236 pp 1-23

[20] Rossi L 2011 LHC Upgrade Plans: Options and Strategy CERN-ATS-2011-257 pp 1-6

[21] Peskin M E 2013 Comparison of LHC and ILC Capabilities for Higgs Boson Coupling Measurements arXiv:1207.2516 [hep-ph] (3) p 18

[22] Klute M et al 2013 Measuring Higgs couplings at a Linear Collider arXiv:1301.1322 [hep-ph] (2) pp 1-4

[23] Tian J and Fujii K 2013 Summary of Higgs coupling measurements with staged running of ILC at 250 GeV, 500 GeV and 1 TeV LC-REP-2013-021 pp 1-8

[24] Simon F, Szalay M and Roloff P 2013 Combined Fits of CLIC Higgs Results for the Snowmass Process LCD-Note-2013-012 pp 1-8

[25] Thomson A 2013 CLIC Workshop 2013 [PowerPoint presentation] ECAL Simulation Studies Overview (Zurich) 28 January - 1 February 2013 [online] Available at: <http://indico.cern.ch/event/204269/session/18/material/slides/1?contribId=202> [Accessed 25/3/2014]

[26] ILD Concept Group 2012 *INTERNATIONAL LARGE DETECTOR* vol 1 pp 1-212

[27] Münnich A and Sailer A 2012 The CLIC_ILD_CDR Geometry for the CDR Monte Carlo Mass Production LCD-Note-2011-002 pp 1-15

[28] Kawagoe K 2011 5th ILD Workshop [PowerPoint presentation] ECAL review (Orsay) 23-25 May 2011 [online] Available at: <http://agenda.linearcollider.org/materialDisplay.py?contribId=10&sessionId =2&materialId=slides&confId=4901> [Accessed 25/3/2014]

[29] Laštovička T 2011 Light Higgs Production and Decays to Pairs of Bottom and Charm Quarks at 3 TeV LCD-Note-2011-036 pp 1-16

[30] Thomson M 2012 *Standard Model Higgs Physics* [PowerPoint presentation] Linear Collider Town Meeting. (Paris) May

[31] Denner A et al 2011 Standard model Higgs-boson branching ratios with uncertainties *The European Physical Journal* **C 71** p 1753

[32] Deutsches Elektronen-Synchrotron DESY 2014 ILC Soft [online] Available at: < http://ilcsoft.desy.de/portal/> [Accessed 25/3/2014]
[33] https://svnsrv.desy.de/viewvc/PandoraPFANew/PandoraPFANew/
[34] Gaede F, Krämer T and Wendt O 2007 Event Reconstruction with MarlinReco at the ILC arXiv:physics/0702171 [physics.ins-det] pp 1-6
[35] Deutsches Elektronen-Synchrotron DESY 2014 MarlinReco A Marlin based Reconstruction Package for the ILC [online] Available at: <http://ilcsoft.desy.de/MarlinReco/current/doc/manual_html/manual.html> [Accessed 25/3/2014]
[36] Marshall J, M´unnich and Thomson A 2012 Particle Flow Performance at CLIC LCD-Note-2011-028 pp 1-22
[37] Thomson A Particle Flow Calorimetry at the ILC pp 1-10 [online] Available at: <http://www.hep.phy.cam.ac.uk/ thomson/publications/hsw06.pdf> [Accessed 25/3/2014]
[38] Thomson A 2009 Particle Flow Calorimetry and the PandoraPFA Algorithm arXiv:0907.3577 [physics.ins-det] pp 1-37